Available online at www.sciencedirect.com
SCIENCE DIRECT
Journal of Solid State Chemistry 179 (2006) 1369–1374
JOURNAL OF SOLID STATE CHEMISTRY
www.elsevier.com/locate/jssc

# Combined powder neutron and X-ray diffraction study of charge and orbital order in $Bi_{0.75}Sr_{0.25}MnO_3$

R.J. Goff[a,b], J.P. Attfield[a,*]

[a]Centre for Science at Extreme Conditions, University of Edinburgh, Erskine Williamson Building, King's Buildings, Mayfield Road, Edinburgh EH9 3JZ, UK
[b]Department of Chemistry, University of Cambridge, Lensfield Road, Cambridge CB2 1EW, UK

Received 4 November 2005; received in revised form 19 January 2006; accepted 27 January 2006
Available online 28 February 2006

**Abstract**

The room temperature structure of $Bi_{0.75}Sr_{0.25}MnO_3$ has been fitted to high-resolution synchrotron X-ray and time-of-flight neutron powder diffraction data. Constrained structural models were refined using a $(\frac{1}{2}00)$ *Pn*11 supercell ($a = 11.0286(2)$ Å, $b = 7.7351(1)$ Å, $c = 5.53419(9)$ Å, and $\alpha = 89.894(1)^\circ$) of the underlying *Pnma* perovskite structure. The best-fit model evidences a 3:1 $Mn^{3+}/Mn^{4+}$ charge ordering with only 30% of the ideal separation of bond valence sums. An ordered intergrowth of antiferro-orbitally ordered ($LaMnO_3$ type) and charge and ferro-orbitally ordered ($YBaMn_2O_6$ type) blocks is observed. Off-centre Bi/Sr displacements are ferroelectrically ordered in this model.


*Keywords:* Charge order; Orbital order; Manganite perovskites; X-ray diffraction; Neutron diffraction

## 1. Introduction

The physics of manganite perovskites has been studied intensively in recent years following the discovery of colossal magnetoresistances in many compositions based on doped $LaMnO_3$ [1]. These materials show an unprecedented range of couplings between Mn spin, charge and lattice degrees of freedom. It is now established that several ground states are possible for doped manganites, principally the itinerant ferromagnetic and insulating charge ordered antiferromagnetic states, and these often coexist over a range of length scales [2].

The charge ordered (CO) ground state is most easily observed in half-doped manganites such as $La_{0.5}Ca_{0.5}MnO_3$. The first model for this CO phase was proposed by Goodenough [3] after the magnetic structure had been found to be the complex CE-type, with ferromagnetic couplings along zig-zag chains [4]. The model assumed that localised $Mn^{3+}$ and $Mn^{4+}$ states order in alternate planes (''stripes''). Orbital ordering (OO) results from the Jahn–Teller distortion of the high spin $3d^4$ $Mn^{3+}$ configuration, and the resulting superexchange interactions are consistent with the observed CE-type spin structure. This model has been confirmed in $Pr_{0.5}Ca_{0.5}MnO_3$ by a recent refinement using high-resolution powder X-ray and neutron diffraction data [5]. Similar methods have been used to determine the CO and OO in $TbBaMn_2O_6$ [6] and $YBaMn_2O_6$ [7,8], and here, in $Bi_{0.75}Sr_{0.25}MnO_3$.

Perovskite manganites can also be synthesised with $Bi^{3+}$ cations on the A sites and the $6s^2$ lone pair on the $Bi^{3+}$ can affect the structure and physical properties of the material. This is seen in the multiferroic (ferromagnetic and ferroelectric) behaviour of $BiMnO_3$, [9,10] and in the high charge ordering temperature $T_{CO} = 525$ K in $Bi_{0.5}Sr_{0.5}MnO_3$ [11]. Phase coexistence has been found in $Bi_{0.5}Sr_{0.5}MnO_3$ down to 1.5 K [12,13] with the majority phase (55%) showing CE-type antiferromagnetic order and the minority phase (45%) A-type antiferromagnetic order. The majority phase showed a $(\frac{1}{2}00)$ lattice modulation but only the average (*Pnma* symmetry) structure was refined because of the phase coexistence. The charge and orbital order is found to be stable to magnetic fields in excess of 40 T at 4 K [14]. Theoretical studies [15] have suggested

*Corresponding author. Fax: +44 131 650 4743.
*E-mail address:* j.p.attfield@ed.ac.uk (J.P. Attfield).

0022-4596/$ - see front matter © 2006 Elsevier Inc. All rights reserved.
doi:10.1016/j.jssc.2006.01.050

that when the $Bi^{3+}$ $6s^2$ lone pair is weakly screened, this lone pair can hybridise with the O $2p$ orbitals reducing the mobility of the Mn $e_g$ electrons through Mn–O–Mn bridges [16] thus increasing the charge ordering temperature.

Electron microscopy experiments on $Bi_{1-x}Sr_xMnO_3$ ($x = \frac{1}{2}, \frac{2}{3}$)[14] have found an ordering of double 'stripes' of $Mn^{3+}$ with double ($x = \frac{1}{2}$) or quadruple ($x = \frac{2}{3}$) stripes of $Mn^{4+}$ (2:2 and 2:4 ordering, respectively), instead of the conventional 1:1 or 1:2 ordering [17]. Similar double stripe ordering was also observed with a $(\frac{1}{2}\frac{1}{2}0)$ lattice modulation in $Bi_{0.67}Sr_{0.33}MnO_3$ based on an *Imma* unit cell [18]. Diffraction experiments on the solid solution $Bi_{1-x}Sr_xMnO_3$ have found the lattice to be triclinic for $x = 0$, 0.1 and monoclinic for $x = 0.2$, 0.3, $\frac{1}{3}$ based on the cubic perovskite unit cell [19]. These triclinic and monoclinic unit cells can also be described as monoclinic and orthorhombic by reorienting the unit cells [20].

Previous work on $Bi_{0.75}Sr_{0.25}MnO_3$ has found charge ordering at an unusually high $T_{CO} \approx 600$ K, [21,22] ~75 K higher than that in the corresponding half-doped phase $Bi_{0.5}Sr_{0.5}MnO_3$. This unusual behaviour shows the importance of the $Bi^{3+}$ $6s^2$ lone pair in these systems. The space group symmetry above $T_{CO}$ was reported as *Pnma*. A lattice modulation of $(0\frac{1}{2}\frac{1}{2})$ was observed in the CO phase by electron, X-ray and neutron powder diffraction [23], however only an average crystal structure in the higher symmetry space group *Imma* was reported. This behaviour contrasts strongly with that observed in $Bi_{0.75}Ca_{0.25}MnO_3$, where CO does not occur [24]. $Bi_{0.75}Sr_{0.25}MnO_3$ orders antiferromagnetically at 120 K, but the spin structure cants towards a ferromagnetic state in applied fields [25]. Here, we report a refinement of the room temperature $Bi_{0.75}Sr_{0.25}MnO_3$ superstructure. No refinements of charge or orbitally ordered superstructures have previously been reported for (Bi,Sr)$MnO_3$ phases.

## 2. Experimental

A polycrystalline sample of $Bi_{0.75}Sr_{0.25}MnO_3$ was prepared by mixing stoichometric amounts of $MnO_2$, $SrCO_3$ and $Bi_2O_3$ and heating under flowing $O_2$ for two days at 1000 °C. The sample was then reground and heated in air for a further 3 days at 1000 °C.

High-resolution X-ray diffraction patterns were recorded on ID31, ESRF, Grenoble for 10 h from a 0.2 mm capillary in a $2\theta$ range 0–70° at 300 K. Neutron diffraction patterns were recorded on HRPD, ISIS, UK from a 8 mm cylindrical vanadium can for 11 h at 300 K. The X-ray data and neutron diffraction from the backscattering ($2\theta = 168°$) and the $2\theta = 90°$ banks of HRPD were fitted simultaneously using the GSAS software package [26]. The minimum $d$-spacing used in the refinement was 0.7 Å. Additional diffraction contributions from $Mn_3O_4$ (7%, from the neutron fit) and $Bi_2O_3$ (1%) were also fitted.

## 3. Results

The presence of excess $Mn_3O_4$ suggests that some Bi has been lost by volatilisation during the synthesis of the $Bi_{1-x}Sr_xMnO_3$ sample with nominal $x = 0.25$, and this is confirmed by the refined value of $x = 0.28(1)$. This is comparable to the value of $x = 0.29(4)$ obtained by analytical electron microscopy for a sample prepared at 950 °C [25]. The CO and OO superstructure is robust to this slight deviation from the ideal $Bi_{0.75}Sr_{0.25}MnO_3$ composition.

Many superstructure peaks were observed in the X-ray and neutron profiles, and these were indexed by a principal $(\frac{1}{2}00)$ modulation of the *Pnma* unit cell. Additional shoulders on a few diffraction peaks are consistent with a further $(0\frac{1}{2}0)$ periodicity, but too little diffraction intensity was present to allow this modulation to be fitted. The principal $(\frac{1}{2}00)$ modulation contrasts with the $(0\frac{1}{2}\frac{1}{2})$ vector reported in previous X-ray and neutron diffraction experiments on $Bi_{0.75}Sr_{0.25}MnO_3$ [23] but is the same as that seen by electron diffraction from $Bi_{0.67}Sr_{0.33}MnO_3$ [18]. Peak broadenings or splittings showed that the lattice is metrically monoclinic with **a** being the unique axis (keeping the *Pnma* setting). The highest allowed space group symmetry for this monoclinic $2a \times b \times c$ supercell is the acentric group $Pn11$.

Full $2a \times b \times c$ superstructure refinements in $Pn11$ were unstable due to the large number of independent coordinates (62), and so a series of constrained models were tested. Starting coordinates were taken from a fit of the average *Pnma* structure. Four independent $A$ cation (Bi/Sr) sites are present in the cell. Initial fits to the X-ray data showed that these could be modelled satisfactorily by constraining the Bi and Sr $x$ and $z$ values to be the same, but refining separate $y$ coordinates for the $Bi^{3+}$ and $Sr^{2+}$ ions to model possible 'off-centre' displacements of $Bi^{3+}$. Bi/Sr $x$ values were constrained to have *Pnma* pseudosymmetry, while two independent $z$'s were refined.

The $Pn11$ supercell contains four independent Mn sites that define 'stripes' in the $ac$ plane. The Mn ions were fixed at their ideal *Pnma* coordinates. Charge ordering in $Bi_{0.75}Sr_{0.25}MnO_3$ is expected to produce three stripes of $Mn^{3+}$ (sites Mn(1)–Mn(3)) separated by single stripes of $Mn^{4+}$ (Mn(4)). These layers are stacked along **b** such that blocks of two $Mn^{3+}$ stripes (Mn(1) and Mn(2)) are stacked above each other in successive layers, whereas blocks of alternating $Mn^{3+}$ (Mn(3)) and $Mn^{4+}$(Mn(4) stripes are stacked at the other two positions, as shown Fig. 1. For convenience we refer to these as the Mn(1)–Mn(2) block (containing only $Mn^{3+}$ states) and the Mn(3)–Mn(4) block (containing alternating $Mn^{3+}$ and $Mn^{4+}$ stripes).

Jahn–Teller distortions typically lead to elongation of one trans pair of Mn–O bonds associated with the local $3d_{z^2}$ orbital in the $Mn^{3+}O_6$ octahedra. These distortions are usually ordered cooperatively such that none of the Mn–O–Mn bridges contain two $3d_{z^2}$ orbitals directed towards the same bridging oxygen. These considerations

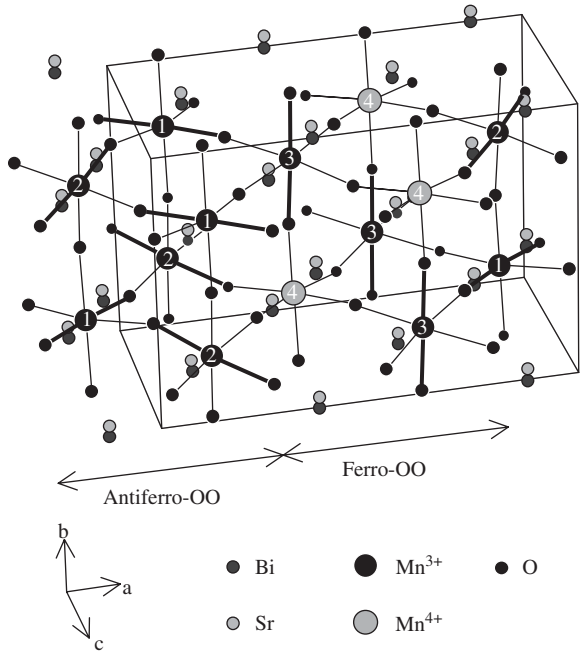


Fig. 1. The refined structural model for $Bi_{0.75}Sr_{0.25}MnO_3$ at 300 K in space group *Pn*11. The elongated Mn–O bonds arising from Jahn–Teller distortions are shown as thickened lines. Antiferro-orbitally ordered ($LaMnO_3$ type) and ferro-orbitally ordered ($YBaMn_2O_6$ type) blocks are labelled.

give two OO schemes for each of the above blocks. In the Mn(1)–Mn(2) block, the $d_{z^2}$ orbitals at both $Mn^{3+}$ sites may lie in the *ac* plane (*ac–ac* order), or else the distortions lie in this plane at one site, but in the perpendicular $\pm\mathbf{b}$ direction at the other site (*ac–b* order). The Mn(3)–Mn(4) block contains alternating $Mn^{3+}$ and $Mn^{4+}$ states and the orbital disortions at the Mn(3) site may lie in the *ac* plane (*ac* order) or in the $\pm\mathbf{b}$ direction (*b* order). The two OO schemes possible for each block result in four OO models for the overall structure. Each of these was tested by constraining the oxygen displacements corresponding to the $3d_{z^2}$ elongations to allow a locally centric distortion superimposed on the underlying *Pnma* structure. The fitting residuals for the four models are shown in Table 1.

The four OO models all give acceptable fits to the powder neutron and X-ray data. There is no significant difference between the X-ray fitting residuals. However, Model 2 gave a slightly better neutron fit leading to a lower overall $\chi^2$. The greatest discrimination between models comes from the fits to the neutron superstructure reflections, which have odd *h* values when indexed on the $2a \times b \times c$ supercell. Model 2 gives the best fit to these reflections, although the $R_{F^2}(N, h\ \text{odd})$ values are high because of the low intensities of the superstructure peaks. Furthermore, inspection of the bond distances from the four refinements showed that only Model 2 contained clear Jahn–Teller distortions at the $Mn^{3+}$ sites. The magnitudes of the refined OO distortions were very small for the other three models. Hence, Model 2 is taken to be the most probable model for CO and OO in $Bi_{0.75}Sr_{0.25}MnO_3$, as shown in Fig. 1. Refinement results are given in Tables 2–4, and the profile fits are shown in Fig. 2.

Table 1
Comparison of the four orbital ordering models for $Bi_{0.75}Sr_{0.25}MnO_3$

| Model | 1 | 2 | 3 | 4 |
|---|---|---|---|---|
| Mn(1)–Mn(2) | *ac–ac* | *ac–ac* | *ac–b* | *ac–b* |
| Mn(3)–Mn(4) | *ac* | *b* | *ac* | *b* |
| $\chi^2$ | 8.48 | 8.30 | 8.62 | 8.46 |
| $R_{wp}(N)$ (%) | 8.26 | 8.13 | 8.36 | 8.25 |
| $R_{wp}(X)$ (%) | 13.73 | 13.76 | 13.74 | 13.73 |
| $R_{F^2}(N)$ (%) | 15.32 | 15.24 | 15.16 | 15.32 |
| $R_{F^2}(X)$ (%) | 12.11 | 12.26 | 12.24 | 12.21 |
| $R_{F^2}(N, h\ \text{odd})$ (%) | 58.21 | 53.90 | 65.95 | 58.34 |
| $R_{F^2}(X, h\ \text{odd})$ (%) | 63.65 | 61.80 | 62.35 | 63.65 |

The orbital ordering scheme within the Mn blocks are shown, followed by the goodness-of-fit and the residuals for the combined fits to the 300 K neutron and X-ray profiles.

Table 2
Refined atomic coordinates for $Bi_{0.75}Sr_{0.25}MnO_3$ at 300 K in space group *Pn*11

| Atom | *x* | *y* | *z* |
|---|---|---|---|
| Bi(1) | −0.1258(8) | 0.0018(5) | 0.0133(10) |
| Sr(1) | −0.1258(8) | 0.0438(9) | 0.0133(10) |
| Bi(2) | 0.1242(8) | 0.0018(5) | 0.5022(10) |
| Sr(2) | 0.1242(8) | 0.0438(9) | 0.5022(10) |
| Bi(3) | 0.3742(8) | 0.0018(5) | 0.0133(10) |
| Sr(3) | 0.3742(8) | 0.0438(9) | 0.0133(10) |
| Bi(4) | 0.6242(8) | 0.0018(5) | 0.5022(10) |
| Sr(4) | 0.6242(8) | 0.0438(9) | 0.5022(10) |
| Mn(1) | 0.125 | 0.75 | 0 |
| Mn(2) | 0.875 | 0.75 | 0.5 |
| Mn(3) | 0.375 | 0.75 | 0.5 |
| Mn(4) | 0.625 | 0.75 | 0 |
| O1(1) | −0.1241(14) | 0 | 0.5532(3) |
| O1(2) | 0.1259(14) | 0 | −0.0532(3) |
| O1(3) | 0.3759(14) | 0.0104(11) | 0.5532(3) |
| O1(4) | 0.6259(14) | −0.0104(11) | −0.0532(3) |
| O2(1) | −0.0181(4) | 0.7808(1) | 0.2007(7) |
| O2(2) | 0.5086(4) | 0.7808(1) | 0.2773(7) |
| O2(3) | 0.2412(4) | 0.2192(1) | 0.2773(7) |
| O2(4) | 0.7679(4) | 0.2192(1) | 0.2007(7) |
| O2(5) | 0.2460(6) | 0.7808(1) | 0.2753(10) |
| O2(6) | 0.7460(6) | 0.7808(1) | 0.2753(10) |
| O2(7) | 0.0056(6) | 0.2192(1) | 0.2466(10) |
| O2(8) | 0.5040(6) | 0.2192(1) | 0.2666(10) |

The lattice parameters are $a = 11.0286(2)$ Å, $b = 7.7351(1)$ Å, $c = 5.53419(9)$ Å and $\alpha = 89.894(1)^\circ$. The residuals are $\chi^2 = 8.3$, $R_{wp}$ (Bank 1 HRPD) = 7.31%, $R_{wp}$ (Bank 2 HRPD) = 8.48%, and $R_{wp}$ (ID31) = 13.76%. The isotropic thermal parameters *U* are 0.0318(3) $Å^2$ for Bi/Sr, 0.0064(3) $Å^2$ for Mn and 0.0395(3) $Å^2$ for O. The Bi and Sr site occupancies are 0.72(1) and 0.28(1), respectively.

## 4. Discussion

The monoclinic *Pn*11 $2a \times b \times c$ supercell accounts for almost all of the superstructure intensities in the 300 K

Table 3
The refined Mn–O distances (Å) for $Bi_{0.75}Sr_{0.25}MnO_3$ at 300 K for the three pairs of bonds in the given directions, the mean Mn–O bond distances and bond valence sums (BVS) are also given for the four unique Mn sites

| Mn–O distances (Å) | Mn(1) | Mn(2) | Mn(3) | Mn(4) |
|---|---|---|---|---|
| $\pm\mathbf{b}$ | –O1(1),O1(2) | –O1(1),O1(2) | –O1(3),O1(4) | –O1(3),O1(4) |
| | 1.9555(3) | 1.9566(3) | 2.036(8) | 1.876(8) |
| | (*x*2) | (*x*2) | (*x*2) | (*x*2) |
| $\pm(\frac{1}{2}\mathbf{a}+\mathbf{c})$ | –O2(5),O2(7) | –O2(6),O2(7) | –O2(8),O2(5) | –O2(6),O2(8) |
| | 2.040(6) | 1.904(6) | 2.003(7) | 2.040(6) |
| | 2.024(6) | 1.911(6) | 1.904(6) | 1.937(7) |
| $\pm(\frac{1}{2}\mathbf{a}-\mathbf{c})$ | –O2(4),O2(1) | –O2(1),O2(3) | –O2(2),O2(4) | –O2(2),O2(3) |
| | 2.049(5) | 2.046(5) | 1.935(5) | 2.015(5) |
| | 1.945(5) | 2.013(5) | 1.942(5) | 1.938(5) |
| Mean Mn–O | 1.995(5) | 1.965(5) | 1.976(7) | 1.947(7) |
| BVS | 3.12 | 3.39 | 3.29 | 3.58 |

Table 4
The refined Bi–O and Sr–O distances (Å) for $Bi_{0.75}Sr_{0.25}MnO_3$ at 300 K

| Bi(1)–O bond lengths (Å) | | Sr(1)–O bond lengths (Å) | | Bi(2)–O bond lengths (Å) | | Sr(2)–O bond lengths (Å) | |
|---|---|---|---|---|---|---|---|
| –O2(1) | 3.187(7) | –O2(1) | 2.977(8) | –O2(1) | 2.691(5) | –O2(1) | 2.438(8) |
| –O2(4) | 2.299(6) | –O2(4) | 2.073(8) | –O2(3) | 2.456(7) | –O2(3) | 2.246(8) |
| –O2(5) | 2.853(7) | –O2(5) | 2.616(9) | –O2(6) | 3.001(7) | –O2(6) | 2.776(8) |
| –O2(7) | 2.569(8) | –O2(7) | 2.369(9) | –O2(7) | 2.556(8) | –O2(7) | 2.355(10) |
| Mean | 2.727(7) | Mean | 2.509(9) | Mean | 2.676(7) | Mean | 2.454(9) |
| –O1(1) | 2.547(6) | –O1(1) | 2.570(6) | –O1(1) | 2.753(14) | –O1(1) | 2.774(14) |
| –O1(1) | 2.988(6) | –O1(1) | 3.006(6) | –O1(2) | 3.073(6) | –O1(2) | 3.093(6) |
| –O1(2) | 2.800(14) | –O1(2) | 2.821(14) | –O1(2) | 2.461(6) | –O1(2) | 2.484(6) |
| –O1(4) | 2.765(14) | –O1(4) | 2.795(14) | –O1(3) | 2.791(14) | –O1(3) | 2.802(14) |
| Mean | 2.775(10) | Mean | 2.798(10) | Mean | 2.770(10) | Mean | 2.788(10) |
| –O2(1) | 2.324(7) | –O2(1) | 2.572(8) | –O2(1) | 2.860(6) | –O2(1) | 3.066(7) |
| –O2(3) | 2.849(6) | –O2(3) | 3.106(6) | –O2(4) | 2.719(6) | –O2(4) | 2.987(7) |
| –O2(6) | 2.649(8) | –O2(6) | 2.869(8) | –O2(5) | 2.512(7) | –O2(5) | 2.743(9) |
| –O2(7) | 2.954(7) | –O2(7) | 3.203(8) | –O2(7) | 2.941(8) | –O2(7) | 3.190(8) |
| Mean | 2.694(7) | Mean | 2.938(8) | Mean | 2.758(7) | Mean | 2.997(8) |
| Overall mean | 2.732(8) | Overall mean | 2.748(9) | Overall mean | 2.735(8) | Overall mean | 2.746(9) |
| **Bi(3)–O bond lengths (Å)** | | **Sr(3)–O bond lengths (Å)** | | **Bi(4)–O bond lengths (Å)** | | **Sr(4)–O bond lengths (Å)** | |
| –O2(2) | 2.833(6) | –O2(2) | 2.594(8) | –O2(2) | 3.022(6) | –O2(2) | 2.799(7) |
| –O2(3) | 2.669(6) | –O2(3) | 2.477(7) | –O2(4) | 2.848(8) | –O2(4) | 2.669(8) |
| –O2(6) | 2.853(7) | –O2(6) | 2.616(9) | –O2(5) | 3.001(7) | –O2(5) | 2.776(8) |
| –O2(8) | 2.617(8) | –O2(8) | 2.421(8) | –O2(8) | 2.505(8) | –O2(8) | 2.300(9) |
| Mean | 2.743(7) | Mean | 2.527(8) | Mean | 2.844(7) | Mean | 2.636(8) |
| –O1(2) | 2.763(14) | –O1(2) | 2.784(14) | –O1(1) | 2.790(14) | –O1(1) | 2.810(14) |
| –O1(3) | 2.548(6) | –O1(3) | 2.560(6) | –O1(3) | 2.754(14) | –O1(3) | 2.765(14) |
| –O1(3) | 2.988(6) | –O1(3) | 2.998(6) | –O1(4) | 3.075(6) | –O1(4) | 3.103(6) |
| –O1(4) | 2.802(14) | –O1(4) | 2.831(14) | –O1(4) | 2.463(6) | –O1(4) | 2.496(6) |
| Mean | 2.778(10) | Mean | 2.793(10) | Mean | 2.771(10) | Mean | 2.794(10) |
| –O2(2) | 2.691(7) | –O2(2) | 2.908(8) | –O2(2) | 2.471(6) | –O2(2) | 2.706(7) |
| –O2(4) | 3.201(6) | –O2(4) | 3.431(7) | –O2(3) | 3.048(6) | –O2(3) | 3.289(8) |
| –O2(5) | 2.649(8) | –O2(5) | 2.869(8) | –O2(6) | 2.512(7) | –O2(6) | 2.743(9) |
| –O2(8) | 2.908(7) | –O2(8) | 3.160(8) | –O2(8) | 2.985(8) | –O2(8) | 3.231(8) |
| Mean | 2.862(7) | Mean | 3.092(8) | Mean | 2.754(7) | Mean | 2.992(8) |
| Overall mean | 2.794(8) | Overall mean | 2.804(9) | Overall mean | 2.790(8) | Overall mean | 2.807(9) |

Distances to the four oxygens at $y \approx 0.25$ (top), $y \approx 0$ (centre) and $y \approx -0.25$ (bottom) are shown, with mean values for each set, and the overall mean below.

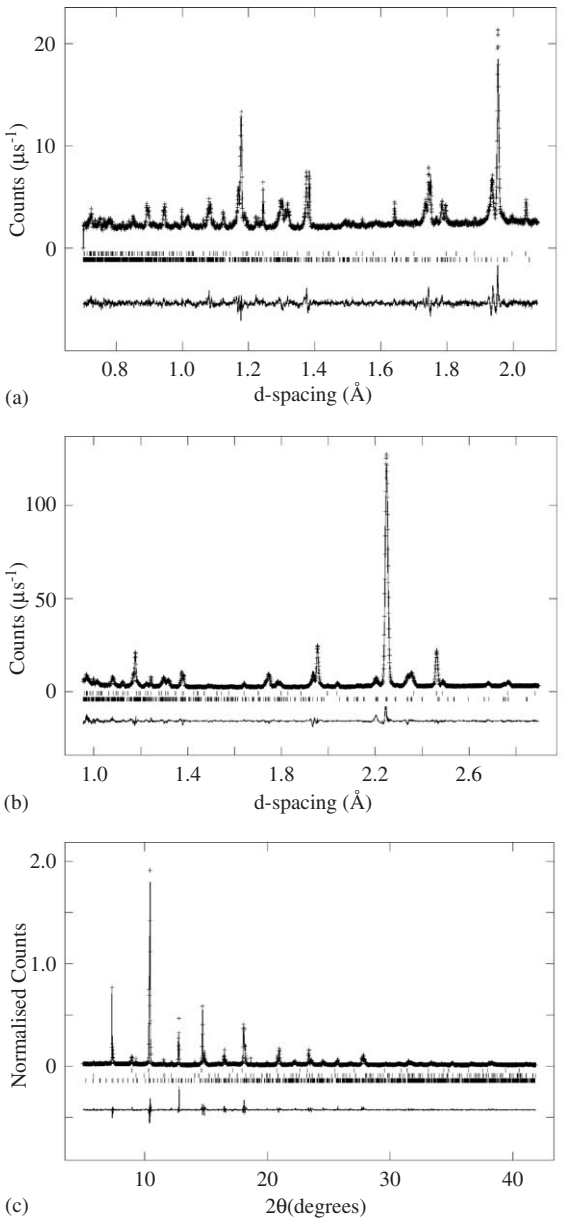


Fig. 2. The observed, calculated and difference plots for fits of the 300 K $Bi_{0.75}Sr_{0.25}MnO_3$ structure in space group *Pn*11 to: (a) HRPD bank 1 neutron data, (b) HRPD bank 2 data, and (c) ID31 X-ray diffraction data. The tick marks (from bottom to top) correspond to; $Bi_{0.75}Sr_{0.25}MnO_3$ , $Mn_3O_4$, and (only in the X-ray fit) $Bi_2O_3$.

neutron and X-ray patterns of $Bi_{0.75}Sr_{0.25}MnO_3$, and so can describe the dominant charge and OO distortions of the structure. However, some additional peak broadenings would require the larger $2a \times 2b \times c$ supercell evidenced by electron microscopy studies of $Bi_{1-x}Sr_xMnO_3$ [17,18] so that further subtle OO distortions may be present in the full triclinic *P*1 supercell. The complexity of the $2a \times b \times c$ acentric monoclinic superstructure has precluded a free refinement of all the coordinates against the present data. One of the four postulated OO models (Model 2) gives a better fit than the others with a plausible magnitude for the orbital distortions, and so is taken to be the best present approximation to the charge and orbitally ordered structure of $Bi_{0.75}Sr_{0.25}MnO_3$.

The postulated charge ordering $Bi_{0.75}Sr_{0.25}MnO_3$ is supported by the Mn–O distances and bond valence sums [27] in Table 3, from which the Mn(1), Mn(2) and Mn(3) sites approximate to $Mn^{3+}$ (BVS's of 3.1–3.4, average = 3.3) and show Jahn–Teller distortions, whereas Mn(4) approximates to $Mn^{4+}$ (BVS = 3.6) and shows no locally centric Jahn–Teller distortion. The BVS values may be influenced by the model constraints, nevertheless, the estimated 30% of the ideal $Mn^{3+}/Mn^{4+}$ charge separation is typical of that observed in other symmetry broken CO oxides such as $Pr_{0.5}Ca_{0.5}MnO_3$ (25%) [5], $YNiO_3$ (30%) [28], and $TbBaFe_2O_5$ (40%) [29].

The CO and OO scheme for $Bi_{0.75}Sr_{0.25}MnO_3$ in Fig. 1 may be described as an ordered intergrowth of two distinctive blocks. In the Mn(1)–Mn(2) blocks of $Mn^{3+}$, the $d_{z^2}$ orbitals lie in the *ac* plane. This gives rise to equal numbers of elongation distortions in two mutually perpendicular directions in the supercell, $\pm(\frac{1}{2}\mathbf{a}+\mathbf{c})$ and $\pm(\frac{1}{2}\mathbf{a}-\mathbf{c})$ (Table 3), corresponding to an antiferro-orbital ordering (AFOO), as found in undoped $LaMnO_3$ [30]. The Mn(3)–Mn(4) blocks contain equal numbers of $Mn^{3+}$ and $Mn^{4+}$ ions. The Mn(3) $d_{z^2}$ orbitals are all parallel to **b**, corresponding to ferro-orbital ordering (FOO). This CO and FOO arrangement is observed in the *A* cation ordered manganite $YBaMn_2O_6$ [7]. The energy balance between AFOO and FOO structures may be small in distorted lattices [8] and has been studied theoretically for half-doped manganites [31]. In the 25% doped structure of $Bi_{0.75}Sr_{0.25}MnO_3$, an ordered intergrowth of double stripes of AFOO $LaMnO_3$-type and FOO $YBaMn_2O_6$-type intergrowths is observed. When projected on the *ac* plane, this will give rise to the characteristic double stripe ordering observed in electron microscopy studies of $Bi_{1-x}Sr_xMnO_3$ materials [17,18]. The structural model deduced for $Bi_{0.67}Sr_{0.33}MnO_3$ from such images in Ref. [18] agrees with the arrangement in Fig. 1, and strongly corroborates our finding that Model 2 is the best structural model out of the four possibilities described above.

The independently refined *y* coordinates for the *A* site cations (Table 2) lead to an offset of 0.325(8) Å between Bi and Sr cations. The resulting Bi–O and Sr–O distances are shown in Table 4. The mean Sr–O distances are longer than the Bi–O average for all four Bi/Sr sites, in keeping with the cationic radii. However, the distances to the oxygens in the planes above ($y \approx 0.25$), coincident with ($y \approx 0$), and below ($y \approx -0.25$) the Bi/Sr cations do not reveal the expected 'off-centre' displacements associated with $Bi^{3+}$. Less-constrained structural refinements and dielectric measurements (if practicable) will be needed to confirm whether $Bi_{0.75}Sr_{0.25}MnO_3$ is ferroelectric as suggested by our acentric refinement model. No separate ferroelectric transition is reported for $Bi_{0.75}Sr_{0.25}MnO_3$, and it is probable that the ferroelectric, charge, and orbital order distortions all occur at the 600 K transition. An additional

antiferromagnetic spin ordering transition is observed at 120 K [25].

The coupling of multiple order parameters (charge, orbital, off-centre, and spin) in $Bi_{0.75}Sr_{0.25}MnO_3$ is similar to the coupling of ferroelectric and ferromagnetic order in $RMn_2O_5$ ($R$ = Tb, Ho, Dy) [32,33], hexagonal $RMnO_3$ perovskites with for example $R$ = Y [34,35] and $BiMnO_3$ [9,10].

In conclusion, the most probable charge and orbital order model for $Bi_{0.75}Sr_{0.25}MnO_3$ has been determined by fits to 300 K powder X-ray and neutron diffraction data. A 3:1 ordering of rows of $Mn^{3+}$ and $Mn^{4+}$ occurs in the *ac* plane with an average 30% valence separation estimated by bond valence sums. An intergrowth of antiferro-orbitally ordered ($LaMnO_3$ type) and charge and ferro-orbitally ordered ($YBaMn_2O_6$ type) blocks is observed. These structural distortions are coupled with off-centre Bi/Sr displacements, and a further ordering of Mn spins occurs below 150 K.

## Acknowledgments

We thank Dr. J.P. Wright and Dr. F. Fauth (ESRF), and Dr. R. Ibberson and Prof. P.G. Radaelli (ISIS) for assistance with data collection, and EPSRC for providing beam time and support for R.J.G.

## References

[1] S. Jin, M. McCormack, T. Tiefel, R. Ramesh, J. Appl. Phys. 76 (1994) 6929.
[2] M. Uehara, S. Mori, C.H. Chen, S.-W. Cheong, Nature 399 (1999) 560.
[3] J.B. Goodenough, Phys. Rev. 100 (1955) 564.
[4] E.O. Wollan, W.C. Koehler, Phys. Rev. 100 (1955) 545.
[5] R.J. Goff, J.P. Attfield, Phys. Rev. B 70 (2004) 140404.
[6] A.J. Williams, J.P. Attfield, Phys. Rev. B 66 (2002) 220405.
[7] A.J. Williams, J.P. Attfield, Phys. Rev. B 72 (2005) 024436.
[8] A.J. Williams, J.P. Attfield, S.A.T. Redfern, Phys. Rev. B 72 (2005) 184426.
[9] A. Moreira dos Santos, S. Parashar, A.R. Raju, Y.S. Zhao, A.K. Cheetham, C.N.R. Rao, Solid State Commun. 122 (2002) 49.
[10] A. Moreira dos Santos, A.K. Cheetham, T. Atou, Y. Syono, Y. Yamaguchi, K. Ohoyama, H. Chiba, C.N.R. Rao, Phys. Rev. B 66 (2002) 064425.
[11] J.L. Garcia-Munoz, C. Frontera, M.A.G. Aranda, A. Llobet, C. Ritter, Phys. Rev. B 63 (2001) 064415.
[12] C. Frontera, J.L. Garcia-Munoz, M.A.G. Aranda, C. Ritter, A. Llobet, M. Respaud, J. Vanacken, Phys. Rev. B 64 (2001) 054401.
[13] C. Frontera, J.L. Garcia-Munoz, A. Llobet, M.A.G. Aranda, C. Ritter, M. Respaud, J. Vanacken, J. Phys.: Condens. Matter 13 (2001) 1071.
[14] C. Frontera, J.L. Garcia-Munoz, M.A.G. Aranda, C. Ritter, A. Llobet, L. Ranno, M. Respaud, J. Vanacken, A.E. Carrillo, A. Calleja, J. Garcia, Appl. Phys. A 74 (2002) S1787.
[15] N.A. Hill, K.M. Rabe, Phys. Rev. B 59 (1999) 8759.
[16] M. Hervieu, A. Maignan, C. Martin, N. Nguyen, B. Raveau, Chem. Mater. 13 (2001) 1356.
[17] C.H. Chen, S.-W. Cheong, H.Y. Hwang, J. Appl. Phys. 81 (1997) 4326.
[18] M. Hervieu, S. Malo, O. Perez, P. Beran, C. Martin, G. Baldinozzi, B. Raveau, Chem. Mater. 15 (2003) 523.
[19] H. Chiba, T. Atou, Y. Syono, J. Solid State Chem. 132 (1997) 139.
[20] H. Chiba, T. Atou, H. Faqir, M. Kikuchi, Y. Syono, Y. Murakami, D. Shindo, Solid State Ionics 108 (1998) 193.
[21] C. Frontera, J.L. Garcia-Munoz, C. Ritter, L. Manosa, X.G. Capadevila, A. Calleja, Solid State Commun. 125 (2003) 277.
[22] J.L. Garcia-Munoz, C. Frontera, M.A.G. Aranda, C. Ritter, A. Llobet, M. Respaud, M. Goiran, H. Rakoto, O. Masson, J. Vanacken, J.M. Broto, J. Solid State Chem. 171 (2003) 84.
[23] C. Frontera, J.L. Garcia-Munoz, M.A.G. Aranda, M. Hervieu, C. Ritter, L. Manosa, X.G. Capadevila, A. Calleja, Phys. Rev. B 68 (2003) 134408.
[24] C. Frontera, J.L. Garcia-Munoz, A.E. Carrill, M. Hervieu, A. Calleja, X.G. Capadevila, M.T. Casais, C. Ritter, Physica B 350 (2004) 48.
[25] J.L. Garcia-Munoz, C. Frontera, M. Respaud, M. Giot, C. Ritter, X.G. Capadevila, Phys. Rev. B 72 (2005) 054432.
[26] A.C. Larson, and R.B. Von Dreele, Los Alomos Nation Laboratory Report No. LAUR 86-748 (1999).
[27] I.D. Brown, The bond valence sums were calculated using the program Valence, J. Appl. Crystallogr. 29 (1996) 479.
[28] J.A. Alonso, J.L. Garcia-Munoz, M.T. Fernandez-Diaz, M.A.G. Aranda, M.J. Martinez-Lope, M.T. Casais, Phys. Rev. Lett. 82 (1999) 3871.
[29] P. Karen, P.M. Woodward, J. Linden, T. Vogt, A. Studer, P. Fischer, Phys. Rev. B 64 (2001) 214405.
[30] J.B. Goodenough, Phys. Rev. 100 (1955) 564.
[31] D.I. Khomskii, K.I. Kugel, Phys. Rev. B 67 (2003) 134401.
[32] L.C. Chapon, G.R. Blake, M.J. Gutmann, S. Park, N. Hur, P.G. Radaelli, S.-W. Cheong, Phys. Rev. Lett. 93 (2004) 177402.
[33] G.R. Blake, L.C. Chapon, P.G. Radaelli, S. Park, N. Hur, S.-W. Cheong, J. Rodriguez-Carvajal, Phys. Rev. B 71 (2005) 214402.
[34] A. Filippetti, N.A. Hill, J. Magn. Magn. Mater. 236 (2001) 176.
[35] M. Fiebig, Th. Lottermoser, D. Frohlich, A.V. Goltsev, R.V. Pisarev, Nature 419 (2002) 818.